Supporting Information

Ultrathin flexible electrochromic device enabled by highly transparent ion conducting films

Hui Gong, Ang Li, Guoxing Fu, Meiyu Zhang, Zilong Zheng, Qianqian Zhang, Kailing Zhou, Jingbing Liu, Hao Wang**

Contents

1. Cross-sectional SEM images of the PVDF polymer matrixes with different thickness.

As shown in Figure S1, the cross-sectional SEM images showed that the PVDF polymer matrixes can achieve the thickness from 16.9 to 32.9 μm.

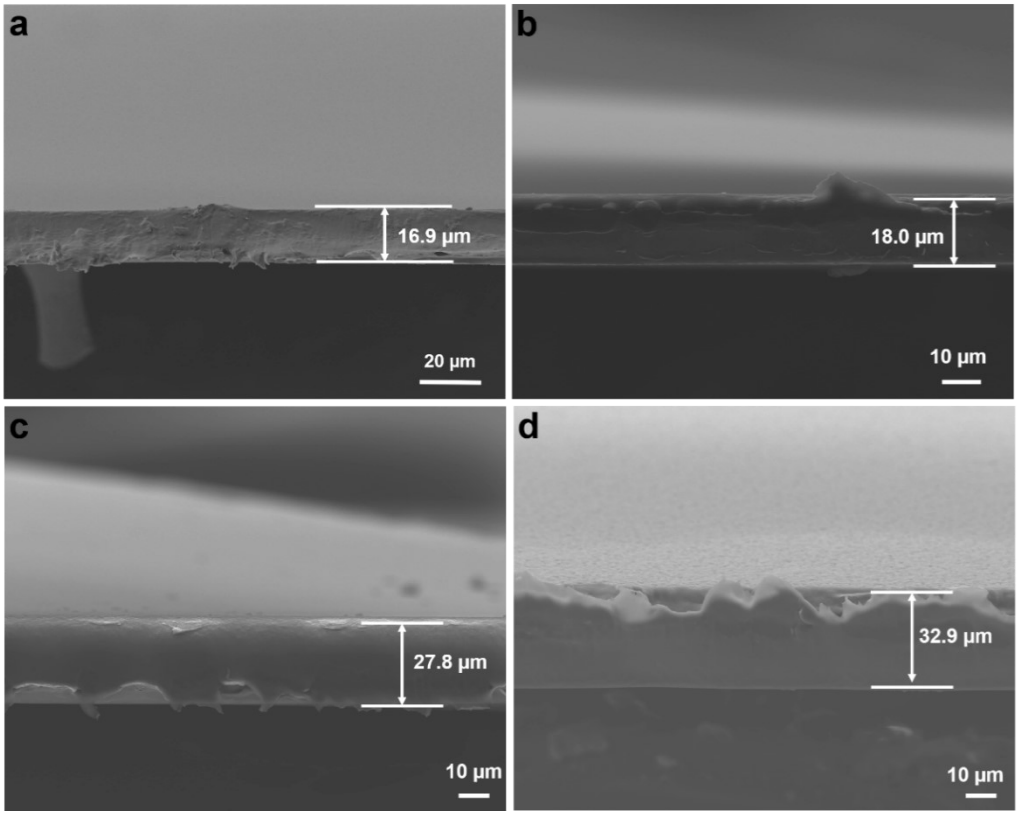

Figure S1. Cross-sectional SEM images of the PVDF polymer matrixes with different thickness.

2. Thermal stability of PVDF polymer matrixes with different thickness

We investigated the thermal stability of PVDF polymer matrixes by exposing the samples at various temperatures for 10 min. As shown in Figure S2, the membranes maintained stable in a wide temperature range and until a slightly shrinkage was observed after heat treatment at 200 ℃, which indicated that the PVDF polymer matrixes had a superior thermal stability.

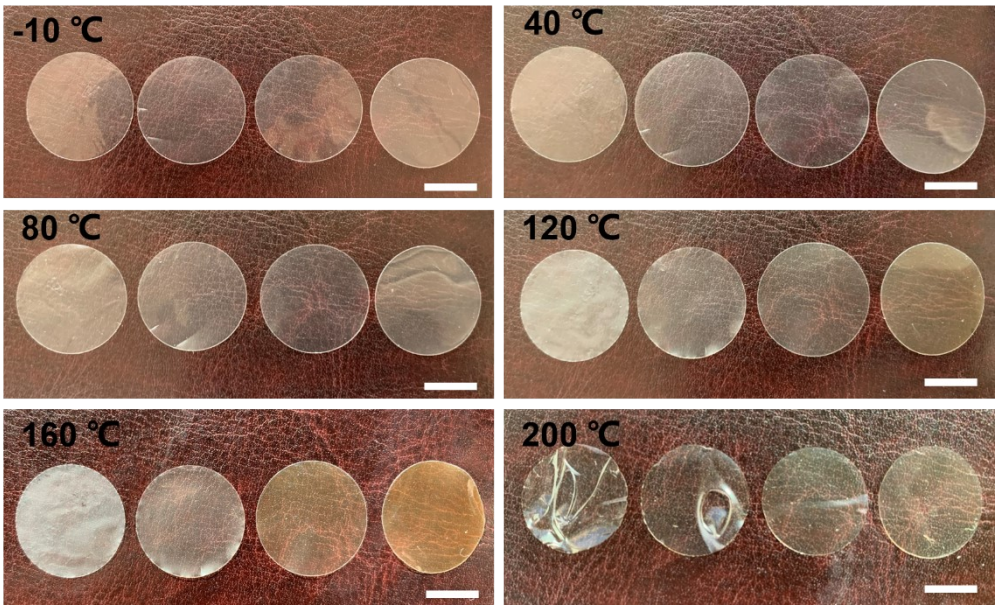

Figure S2. Photographs of the PVDF polymer matrixes at different heat temperatures. Scale Bars:1 cm.

3. The electrolyte wettability of the PVDF polymer matrix

As illustrated in Figure S3, the contact angle of the electrolyte on the surface of the PVDF polymer matrix was ~12.2° after dropping the liquid electrolyte on its surface for 10 s, indicating the favorable affinity between PVDF polymer matrix and the liquid electrolyte.

Figure S3. The contact angle of the PVDF membrane with a thickness of 16.9 μm after adding a drop of the $LiClO_4$-PC electrolyte.

4. The electrochemical stability of the ICF

In order to further demonstrate the electrochemical stability of the ICF, we further recorded the color change of the ICF before and after applying a voltage region from 0 V of 6 V at 10 mV s^{-1}. As shown in Figure S4, it can be seen that the ICF still remain high transparency and no color change even applied a high voltage, compared to its initial state. The ICF demonstrates excellent electrochemical stability.

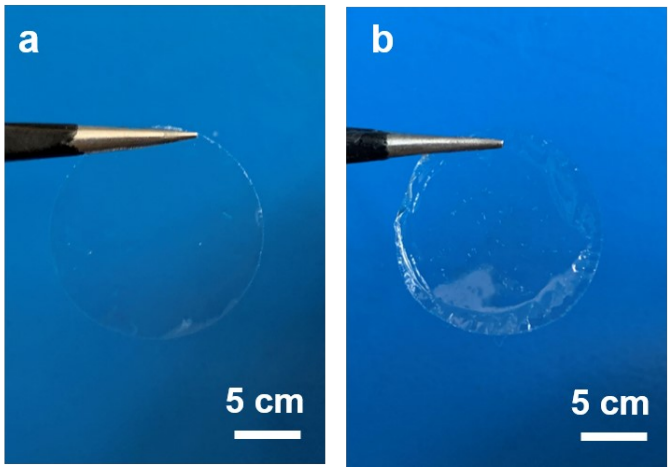

Figure S4**.** The photographs of ICF at initial state (a) and after applying a voltage region from 0 V to 6 V under a sweep rate of 10 mV s^{-1} (b).

5. The surface morphology of PANI electrode

As illustrated Figure S5, the surface morphologies of the PANI electrode deposited on PET/ITO substrate showed a flat and dense surface. The magnified SEM image demonstrated that some particles dispersed on the surface of the electrode, which ascribes to the aggregate phenomenon of PANI.

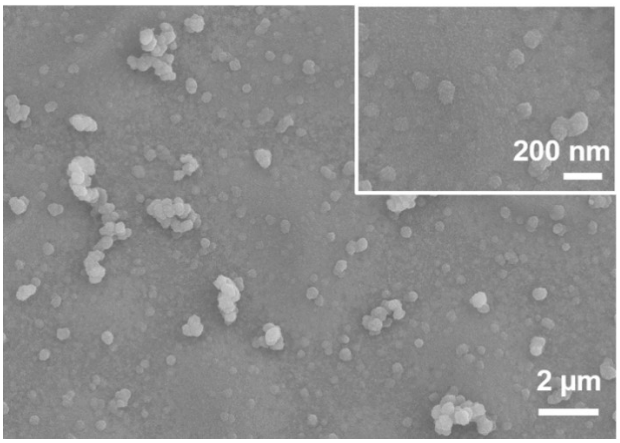

Figure S5. Top-view SEM images and the magnified one (inset) of the PANI electrode.

6. The FTIR of PANI electrode

A Fourier transform infrared (FTIR) spectrum was measured to confirm the component of PANI shown in Figure S6. It can be seen that a strong absorption peak observed at 832 cm^{-1} could be ascribed to the out-of-plane bending of C–H. Two peaks at 1215 and 1372 cm^{-1} were attributed to the stretching of benzenoid ring and C–N stretching mode, respectively. The peaks at 1570 and 1678 cm^{-1} corresponded to the C=N stretching mode and stretching of N–Q–N, respectively. The above results proved that the PANI is the emeraldine salt state [1].

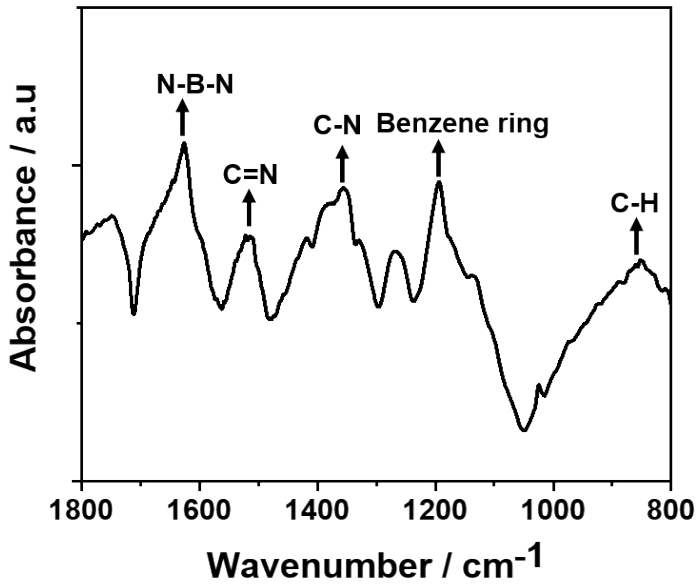

Figure S6. FTIR spectrum of the PANI electrode deposited on PET/ITO substrate.

7. The CV curves of PANI electrode at different scan rates

The cyclic voltammetry (CV) curves were measured in the potential cycled from -0.4 V to 0.8 V by using a three-electrode electrochemical system in 1 M $LiClO_4$-PC electrolyte (Figure S7). The obvious two pair of redox peaks and higher current densities of CV curves at high scan rates could be observed, revealing the remarkable capacitive properties of the PANI electrode [2, 3].

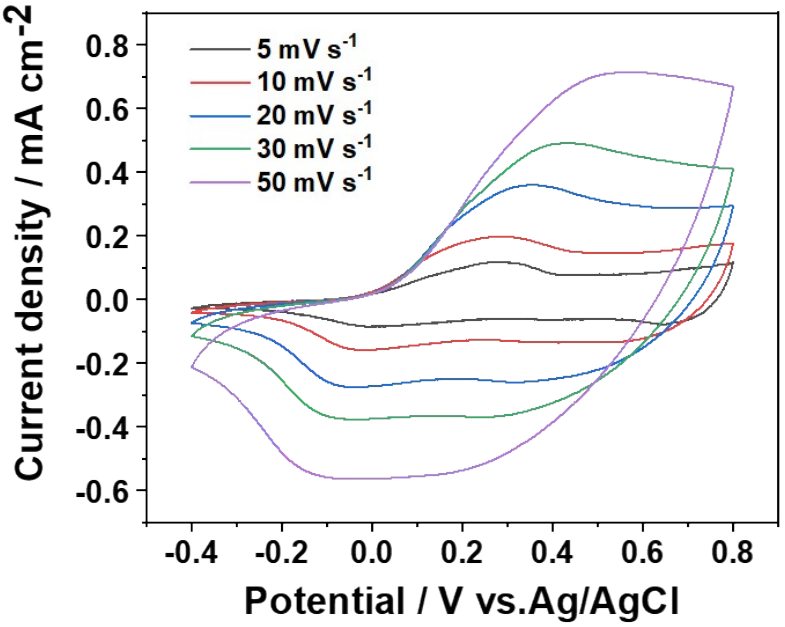

Figure S7. Cyclic voltammograms at various scan rates of the PANI electrode.

8. The oxidation-reduction process of PANI electrode

The PANI electrode was measured in $LiClO_4$-PC electrolyte solution. The simplified redox reaction of the PANI is highlighted in Equations and Figure S8.

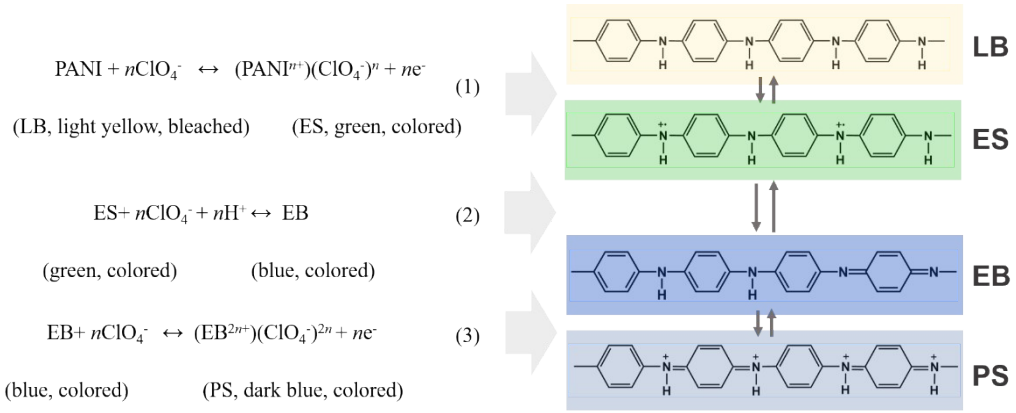

Figure S8. The oxidation-reduction process of PANI electrode

9. Absorbance spectra of PANI electrode under different applied potentials

We investigated the electrochromic properties of the PANI electrode at different applied potentials from -0.4 V to 0.8 V. As shown in Figure S9, the PANI electrode displayed multicolor properties, which change its color from a transparent at -0.4 V to a light-yellow at 0.4 V then to a green state at 0.6 V, and finally a blue at 0.8 V. The corresponding optical changes were recorded by the absorbance spectra. As the applied potential increases from -0.4 to 0.8 V, the absorbance peaks of the sample exhibited a blueshift to the ultraviolet region [4, 5].

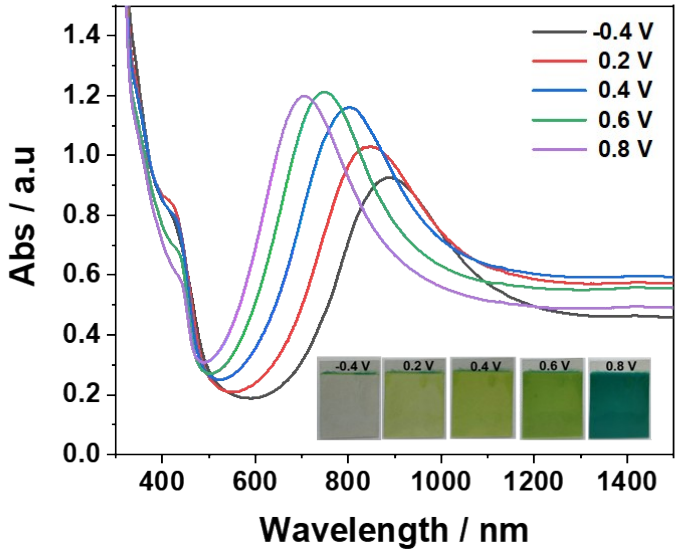

Figure S9. UV-vis transmission spectra of the PANI electrode measured at different potentials.

10. The switching time and color efficiency for PANI electrode

The switching characteristics and kinetics of the PANI electrode were studied under alternating potential between -0.4 and 0.8 V for 15 s. As demonstrated in Figure S10, the response time for coloring and bleaching process at a wavelength of 630nm were found to be about 9.2 s and 4.1 s, respectively. Meanwhile, a coloration efficiency (CE) value of 67.1 cm^2 C^{-1} was obtained (Figure S11).

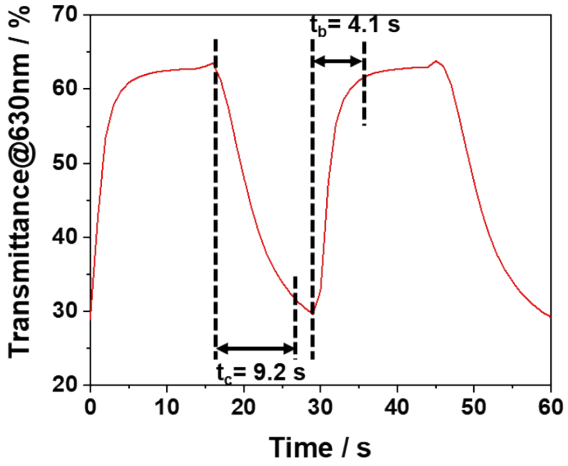

Figure S10. *In-situ* transmittance response by applying alternate potentials of -0.4 V and 0.8 V for 15 s at 630 nm.

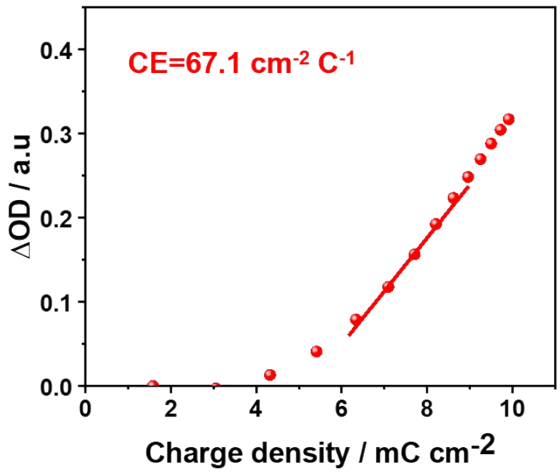

Figure S11. Optical density as a function of the charge density at 550 nm for PANI electrode.

11. Cycling performance of PANI electrode in 1 M $LiClO_4$-PC electrolyte

The cycling performance of PANI film in aqueous and non-aqueous electrolytes, PANI film was measured in 1 M $LiClO_4$-PC via chronoamperometry at -0.4 V and 0.8 V with intervals of 15 s at 630 nm for 500 cycles. As shown in Figure S12, it is obvious that the PANI film shows an initial optical modulation of 53.9%, and retains an initial optical contrast of 58.8% after about 500 cycles.

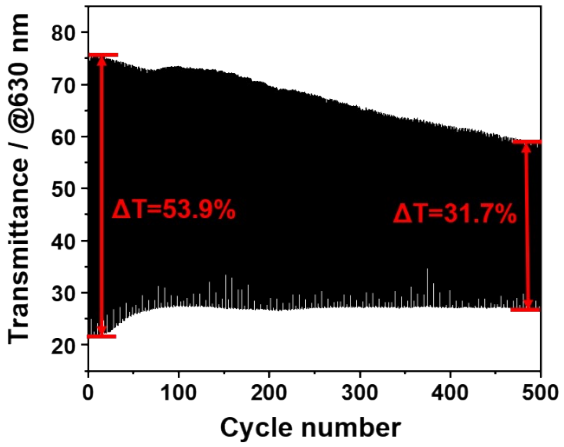

Figure S12. The Cycling stability of PANI electrode tested for 500 cycles.

12. The environmental stability of the ICF-based EC device

In order to estimate the environmental stability of ICF-based EC devices, the device that was stored for about 30 days was measured at different voltages. Compared to the newly assembled ICF-based EC device, the old ICF-based EC device remained stable and still exhibited significant colors change at different voltages even it was stored for about one month (Figure S13a and S13b). Meanwhile, under varied applied voltages of -2.5 to 2.5 V, the device showed obvious transmittance modulation in the wavelength range of 300-1100 nm (Figure S13c). These results demonstrated the excellent environmental stability of the device.

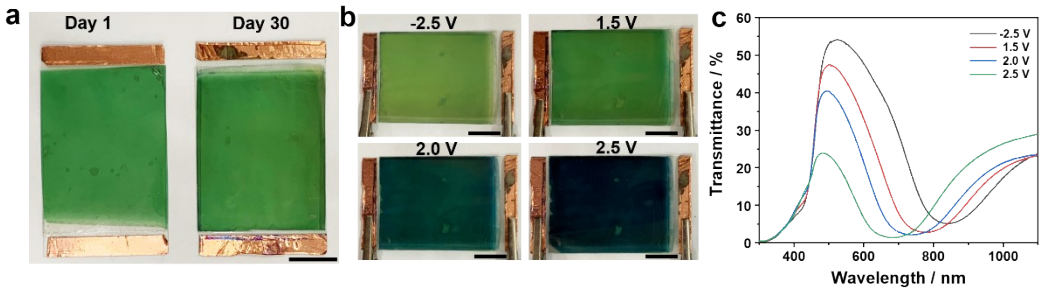

Figure S13. The environmental stability of ICF-based EC device. (a) Photographs of ICF-based EC device of Day 1 and Day 30. Scale bar: 2 cm. (b, c) Photographs of the devices that stored for 30 days (b) and the corresponding transmittance spectra of the device (c) measured at different voltages. Scale bar: 1 cm.

13. Dependence of the degree of polymerization and HOMO-LUMO energy gap

As shown in Figure S14, the most stable molecular configuration with the lowest energy value was evaluated by using the B3LYP/6-31G(d) level of theory (n=1 to 4, where n is the degree of polymerization). The HOMO-LUMO energy gap of PANI was decreased with the degree of polymerization increasing and maintained stable when the degree of polymerization was 4. Such result was consistent of many researchers reports that the aniline tetramer represents the electronic characters of the PANI [6].

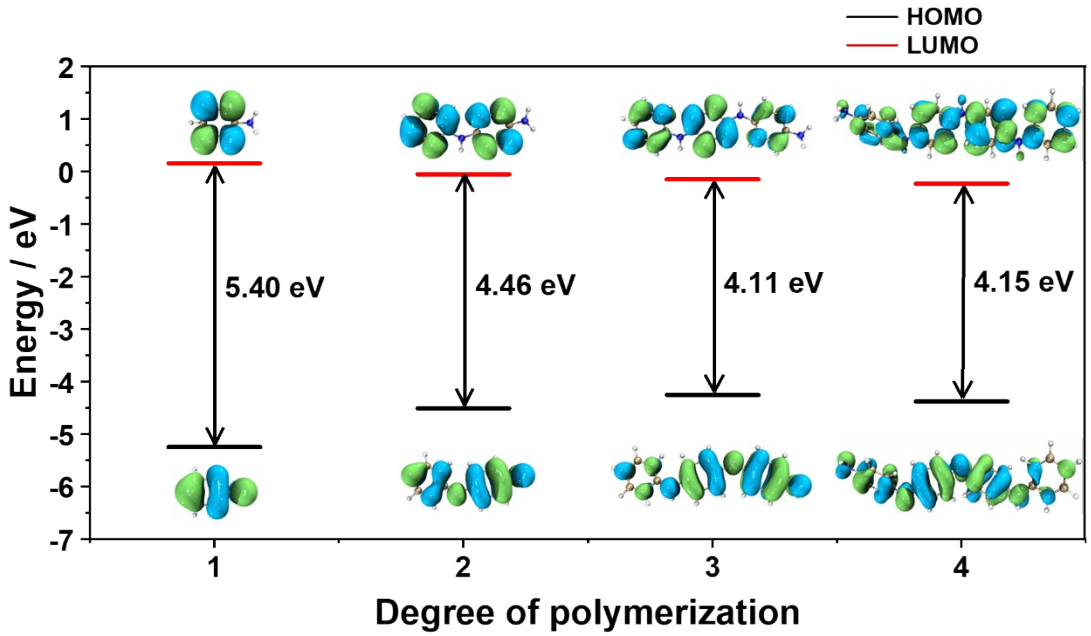

Figure S14. Dependence of the degree of polymerization and HOMO-LUMO energy gap.

14. EIS spectra of the ICF-based EC device at different bending cycles

We carried out the electrochemical impedance spectroscopy (EIS) measurements for the ICF-based EC device at different bending cycles. As shown in Figure S15, it can be seen that all the Nyquist plots are composed of a depressed semicircle at high frequencies and a straight line at low frequencies. Generally, a smaller semicircle demonstrates a smaller charge-transfer resistance. It is found that the device showed larger semicircle in the high frequency region after bending, compared the device without bending. After 500 bending cycling, the device exhibited the largest semicircle. These results indicate that the electron transfer between the ICF and ITO-PET electrode is inhibited during the deformation process. In fact, the device with repeating bending easily results in the poor contact at the interface of ICF and ITO-PET and suffers from unavoidable displacement among adjacent components, which would significantly increase the charge transfer resistance of electrons.

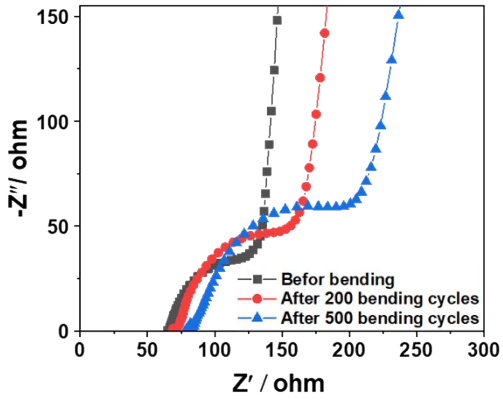

Figure S15. EIS spectra of the ICF-based EC device at different bending cycles

15. Reference

1. W. Guo, Z. Cong, Z. H. Guo, P. Zhang, Y. Chen, W. Hu, Z. L. Wang and X. Pu, *Adv. Funct. Mater*., 2021, **31**, 2104348.

2. X. Huang, Q. Niu, S. Fan and Y. Zhang, *Chem. Eng. J.,* 2021, **417**, 128126.

3. H. Gong, K. Zhou, Q. Zhang, J. Liu, H. Wang and H. Yan, *Sol. Energy Mater. Sol. Cells*, 2020, **215**, 110642.

4. S. Zhang, P. Lei, J. Fu, X. Tong, Z. Wang and G. Cai, *Applied Surface Science,* 2023, **607**, 155015.

5. K. Zhou, H. Wang, J. Jiu, J. Liu, H. Yan and K. Suganuma, *Chem. Eng. J.,* 2018, **345**, 290-299.

6. N. Zohrevand, T. Madrakian, A. Ghoorchian and A. Afkhami, *Electrochim. Acta,* 2022, **427**, 140856.